Temperature-controlled interlayer exchange coupling in strong/weak ferromagnetic multilayers: A thermomagnetic Curie switch

A. F. Kravets,[1,2] A. N. Timoshevskii,[2] B. Z. Yanchitsky,[2] M. A. Bergmann,[1] J. Buhler,[1] S. Andersson,[1] and V. Korenivski[1,*]

[1]*Nanostructure Physics, Royal Institute of Technology, 10691 Stockholm, Sweden*

[2]*Institute of Magnetism, National Academy of Sciences of Ukraine, Vernadsky 36 b, 03142 Kiev, Ukraine*

(Received 28 August 2012; revised manuscript received 12 November 2012; published 14 December 2012)

We investigate interlayer exchange coupling based on driving a strong/weak/strong ferromagnetic trilayer through the Curie point of the weakly ferromagnetic spacer, with exchange coupling between the strongly ferromagnetic outer layers that can be switched on and off, or varied continuously in magnitude by controlling the temperature of the material. We use Ni-Cu alloys of varied composition as the spacer material and model the effects of proximity-induced magnetism and the interlayer exchange coupling through the spacer from first principles, taking into account not only thermal spin disorder but also the dependence of the atomic moment of Ni on the nearest-neighbor concentration of the nonmagnetic Cu. We propose and demonstrate a gradient-composition spacer, with a lower Ni concentration at the interfaces, for greatly improved effective-exchange uniformity and significantly improved thermomagnetic switching in the structure. The reported multilayer materials can form the base for a variety of magnetic devices, such as sensors, oscillators, and memory elements based on thermomagnetic Curie switching.

DOI: 10.1103/PhysRevB.86.214413 PACS number(s): 75.20.En, 75.20.Hr, 75.30.Et, 75.70.Cn

I. INTRODUCTION

Interlayer exchange coupling is one of the key fundamental characteristics of magnetic multilayers,[1,2] important for such large-scale industrial applications as field sensors, magnetic recording, and magnetic random-access memory.[3–6] In many cases it controls the magnetization switching in the system under the influence of external fields[7] or spin-polarized currents.[8–10] The oscillatory interlayer exchange coupling[11–13] [Ruderman-Kittel-Kasuya-Yosida (RKKY)] is due to the conduction electrons mediating the spin transfer between the ferromagnetic layers, and is fixed in fabrication to be positive or negative in magnitude by selecting a suitable thickness of the nonmagnetic metal spacer. Once the coupling is set to be antiparallel, an external switching field is necessary to change the state of the structure to parallel.

It is highly desirable to design multilayer materials where the interlayer exchange coupling is not fixed but rather controllable, on and off, by varying an external physical parameter, such as temperature. One such system is a strong/weak/strong ferromagnetic sandwich (F/f/F), where the weakly ferromagnetic spacer (f) has a lower Curie temperature (T_C) than that of the strong ferromagnetic outer layers (F).[14,15] Heating the structure through the T_C of the spacer exchange-decouples the outer magnetic layers, so their parallel alignment below T_C can be switched to antiparallel above T_C. This switching is fully reversible on cooling through the T_C, as the number of thermal magnons is reduced and the exchange spring in the spacer, aligning the outer F layers, becomes stronger. This action can provide a spin switch or oscillator with intrinsic thermoelectronic control by the Joule heating of a transport current through the structure.[16,17]

The key element in such an F/f/F sandwich is the weakly ferromagnetic spacer f, which should have a T_C that is tunable in fabrication but well defined in operation, and, preferably, a narrow ferromagnetic-to-paramagnetic (P) transition. Diluted ferromagnetic alloys, such as Ni-Cu, with the T_C in the bulk known to be easily tunable to near room temperature,[18,19] represent the natural choice for the spacer material. However, the effects of thermal disorder on the magnetization and exchange coupling in thin-film multilayers are practically unexplored. In particular, the strong exchange at an F/P interface should be expected to suppress the thermal magnons in the spacer, driving the paramagnetic-to-ferromagnetic transition due to the magnetic proximity effect[20,21] and, therefore, result in a gradient of the effective magnetization and interatomic exchange in the spacer,[22,23] as well as critically affecting the interlayer exchange coupling through the spacer. In this work we indeed find a pronounced ferromagnetic proximity effect at F/f(P) interfaces as well as propose and demonstrate experimentally a gradient-spacer design (f*/f/f*), with reduced Ni concentration at the interfaces, which significantly improves the thermomagnetic switching behavior of the multilayer material, and thereby makes it technologically attractive for applications.

Our choice for the diluted ferromagnetic alloy to be used as the spacer material is Ni-Cu. It is considered to be a well-known system, at least in the bulk.[18,19] Our recent detailed studies of sputter-deposited Ni-Cu films[24] confirmed the known general properties, but also revealed some peculiar properties, such as exchange-induced phase separation at high Ni concentration x, above 70 at.% Ni, corresponding to the Curie temperature range above 100 °C. In this work, the concentration range of interest is x(Ni) < 70 at.%, corresponding to the T_C range of 100 °C and below. In fact, the Ni-Cu concentrations with x < 50 at.% are nonmagnetic at all temperatures in the bulk[18,19] or thick films.[25] The situation is quite different in thin-film multilayers, as we show below.

Perhaps the most informative way to investigate the properties of thin spacers (uniform, f, or gradient, f*/f/f*) as it relates to the interlayer exchange is to integrate them into asymmetric trilayers, AF/F/spacer/F, where one of the outer strongly ferromagnetic layers, F, is pinned by an antiferromagnet AF and study the coupling and decoupling of the outer strongly ferromagnetic layers as a function of the spacer composition, thickness, and temperature. The method is not direct as to

measuring the magnetization in the spacer, but is very sensitive and direct when it comes to the exchange interaction of interest.

II. METHODS

Our specific material combinations are based on uniform Ni_xCu_{100-x} (t nm) and gradient Ni_xCu_{100-x}(t nm)/$Ni_{72}Cu_{28}$ (6 nm)/Ni_xCu_{100-x}(t nm) spacers [uniform spacer (us) and gradient spacer (gs), respectively], enclosed by one exchange-pinned and one free Permalloy ($Ni_{80}Fe_{20}$, Py) layer: specifically, $Ir_{20}Mn_{80}$(12 nm)/$Co_{90}Fe_{10}$(2 nm)/Py (2 nm)/us (or gs)/Py (5 nm), hereinafter F_{pin}/Ni_xCu_{100-x}(t nm)/F or F_{pin}/gs/F, respectively. The 2-nm-thick Co-Fe layer is used to improve the pinning at the IrMn/Py interface and does not influence the thermomagnetic transition in the spacer.

The multilayer films were deposited at room temperature on thermally oxidized Si substrates by dc-magnetron sputtering using an AJA Orion multitarget sputtering system. The base pressure in the deposition chamber was $\sim 5 \times 10^{-8}$ Torr and the Ar pressure used during deposition was 5 mTorr. Films of diluted ferromagnetic Ni_xCu_{100-x} alloys of varied composition of 60 nm in thickness were deposited using cosputtering from Ni and Cu targets. The composition of the Ni_xCu_{100-x} films was controlled by setting the corresponding deposition rates of the individual Ni and Cu components, with relevant calibrations obtained by subsequent thickness profilometry and energy-dispersive x-ray analysis.

The magnetic measurements were performed using a vibrating-sample magnetometer in the temperature range of 20–100 °C. Magnetic field was applied in the film plane, along the AF pinning axis.

First-principles calculations of magnetic properties of the spacers in the exchange-coupled multilayers were performed under the assumption that our model system is a Ni/Ni-Cu/Ni trilayer, in which, for purpose of simplicity, the diluted magnetic alloy spacer is enclosed by bulklike fcc Ni [001] (for making the calculations time efficient; qualitatively the same behavior is obtained with Permalloy). Both Ni and Cu atoms in the three-layer structure occupy the sites of the fcc lattice and are distributed randomly within each monolayer in the spacer. The number of atomic monolayers in the spacer is denoted by N_f. The atomic concentration of Ni in the ith monolayer is denoted by c_i. The Ni atoms interact magnetically by the standard isotropic Heisenberg interaction. Cu-Cu and Ni-Cu exchange interactions are neglected since the magnetic moment of Cu is negligible (Cu does not polarize in Ni). The local atomic magnetic moment of Ni, $m_{loc}(z)$, is a function of the number of the nearest-neighbor Ni atoms, z. For obtaining the effective (measurable) magnetic characteristics of the structure we use the mean-field model and take the average Ni magnetic moment to be the same within one monolayer, $m_i = m(z_i)$. The effective magnetic field is[26]

$$H_i = -\sum_j J_j n_{i+j} c_{i+j} m_{i+j}, \qquad (1)$$

where the sum is over monolayers, J_i is the Ni-Ni exchange interaction, and n_i is the coordination number.

The magnetization as a function of temperature was calculated using the mean-field approximation for a lattice-type Hamiltonian, with the standard isotropic Heisenberg exchange interaction between the nickel atoms at sites i, j: $J_{ij}\mathbf{m}_i\mathbf{m}_j$. Taking into account the quasi-one-dimensionality of the problem, all nickel atoms within each atomic monolayer were taken to have the same magnetic moment, such that the exchange and magnetization varied only along the thickness. For a given temperature T, the magnetization of each monolayer is obtained as a solution of the system of nonlinear equations[26] $m_i = L(m_i H_i / k_B T)$, where $L(x)$ is the Langevin function, H_i is the effective magnetic field on the ith nickel site, and k_B is the Boltzmann constant. In this, we include the *ab initio* dependence of the magnitude of the local Ni atomic magnetic moment $|\mathbf{m}| = m_{loc}$ on the nearest-neighbor Cu concentration.

The unknown exchange integrals J_i were obtained for two coordination spheres of the fcc lattice. In this, the total energies of three superstructures of fcc Ni were calculated for the ferromagnetic (F), antiferromagnetic (AF), and antiferromagnetic double[27] (AFD) layer types of magnetic ordering.

With the magnetic energy in the Heisenberg form and assuming the magnetic moment of Ni independent of its direction, the following expressions for the exchange interaction are obtained: $J_1 = (E_F - E_{AF})/8$ and $J_2 = (E_F + E_{AF} - 2E_{AFD})/4$, where E_F, E_{AF}, and E_{AFD} are the full energies of the superstructures.

The total energies of the structures were obtained using the density functional theory approach and the WIEN2K full-potential linearized augmented plane-wave (FLAPW) code.[28] The generalized gradient approximation exchange-correlation potential was the same as in Ref. 29. The radius of the muffin-tin spheres was 2.2 atomic length units. The electron density was computed for 63 k points in the irreducible parts of the first Brillouin zone. The obtained exchange integrals were $J_1 = -6.15$ meV and $J_2 = -17.01$ meV.

III. RESULTS AND DISCUSSION

A. Ni_xCu_{100-x} films

Figure 1 shows the saturation magnetization of 60-nm-thick Ni_xCu_{100-x} films of varied composition normalized to the saturation magnetization of pure Ni. The magnetization vanishes at room temperature for $x \approx 62$ at.%, where the Ni-Cu becomes paramagnetic in the bulk limit (here a single layer 60 nm thick). Figure 1 also shows the saturation magnetization measured at 100 °C, which vanishes at $x \approx 70$ at.%. The ratio of the magnetization at these two temperatures, shown by the triangle symbols in Fig. 1, has a sharp step at 70–74 at.% Ni, suggesting the optimal composition interval for exploiting the ferromagnetic-to-paramagnetic transition in the Ni-Cu alloy films. We show, however, that this composition range must be significantly shifted to lower effective nickel concentrations, if the Ni-Cu spacers are to have sharp thermal transitions in thin-film multilayers.

B. F_{pin}/Ni_xCu_{100-x}(t nm)/F trilayers

Figures 2, 3, 4, and 5 show the key magnetic parameters of the F_{pin}/Ni_xCu_{100-x}(t nm)/F multilayers, measured at room temperature (RT), with the magnetization for the soft F layers

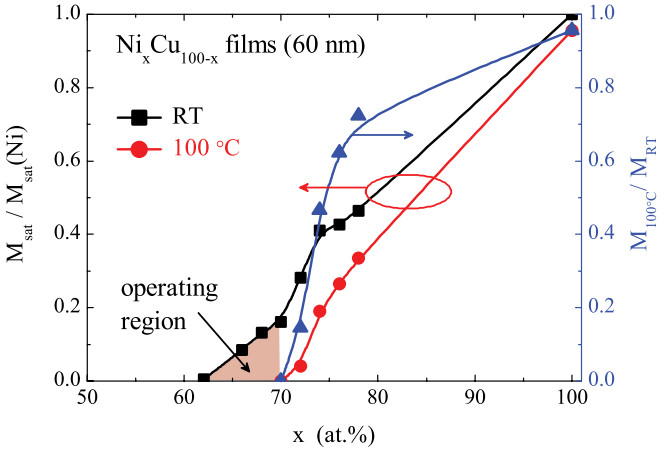

FIG. 1. (Color online) Normalized saturation magnetization of Ni_xCu_{100-x} films as a function of Ni concentration, measured at room temperature (RT) and 100 °C. Triangle symbols show the ratio of the magnetization at the two temperatures, which becomes zero at the boundary of the thermomagnetic operating region. The solid lines are guides to the eye.

always in the film plane and the external in-plane field applied along the AF-pinning axis. Figure 2 shows magnetization loops for the Ni_xCu_{100-x} spacer thickness of 6 nm and x varied in the range from 0 to 72 at.%. For low Ni concentrations ($x < 35$ at.%), due to the absence of any significant magnetic coupling between the free and pinned F layers through the spacer, the magnetization loop consists of two well-separated transitions at approximately zero field and −480 Oe (Fig. 2, green), corresponding to switching of the free Py layer and the pinned ferromagnetic layer, respectively. These loops were separately confirmed to exactly correspond to measured single-layer Py (zero field offset) and a pinned layer of CoFe/NiFe (≈−500 Oe offset). With increasing Ni concentration past $x \approx 35$ at.%, the minor and major loops begin to merge (Fig. 2, blue), indicating an enhanced exchange coupling

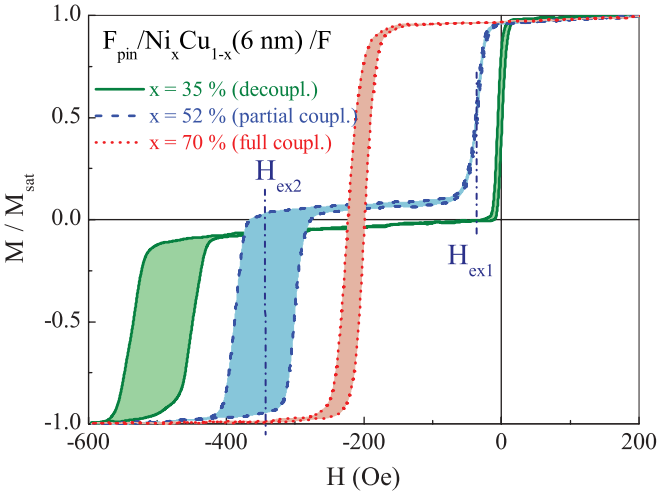

FIG. 2. (Color online) Magnetization loops of F_{pin}/Ni_xCu_{100-x} (6 nm)/F trilayers with spacers having 35, 52, and 70 Ni at.% content. The exchange fields H_{ex1} and H_{ex2} for the free, F, and pinned, F_{pin}, ferromagnetic layers are defined as the midpoints of the respective transitions.

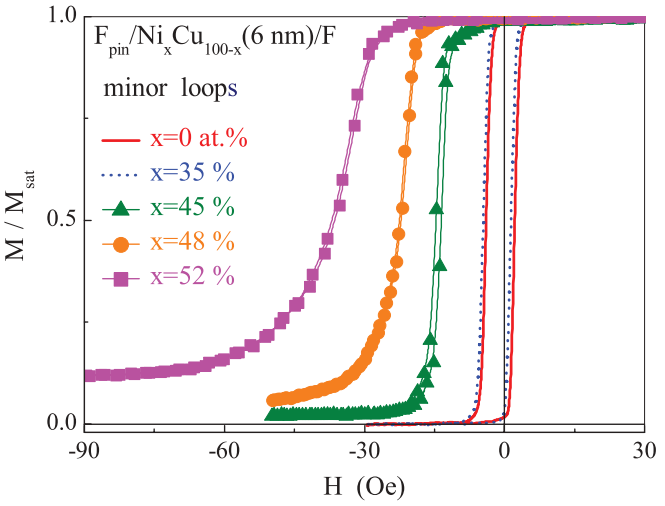

FIG. 3. (Color online) Magnetization minor loops of F_{pin}/Ni_xCu_{100-x}(6 nm)/F trilayers with different Ni-Cu spacer compositions.

between the free and pinned outer layers. The middle points of the two magnetization transitions (minor and major) define the two exchange fields H_{ex1} and H_{ex2}, respectively. As the spacer becomes fully nonmagnetic at low Ni concentrations and does not mediate any exchange coupling, the unpinned Py layer becomes free to switch and $H_{ex1} \to 0$, while H_{ex2} characterizes solely the strength of the AF pinning of the other ferromagnetic layer. Already at $x \approx 52$ at.%, the two transitions merge significantly, indicating a substantial exchange coupling across the spacer. Interestingly, the $x = 52$ at.% composition for single-layer Ni-Cu is nonmagnetic (paramagnetic) at room temperature ($T_C \approx 10$ K) and normally would not be expected to exchange-couple the outer F layers. These data indicate that a ferromagnetic order of significant strength is induced in the paramagnetic spacer on rather long length scales, several nanometers in this case. This induced ferromagnetism couples the outer layers, bringing together the two magnetic transitions, such that H_{ex1} and H_{ex2} merge. Thus, for this geometry, H_{ex1}

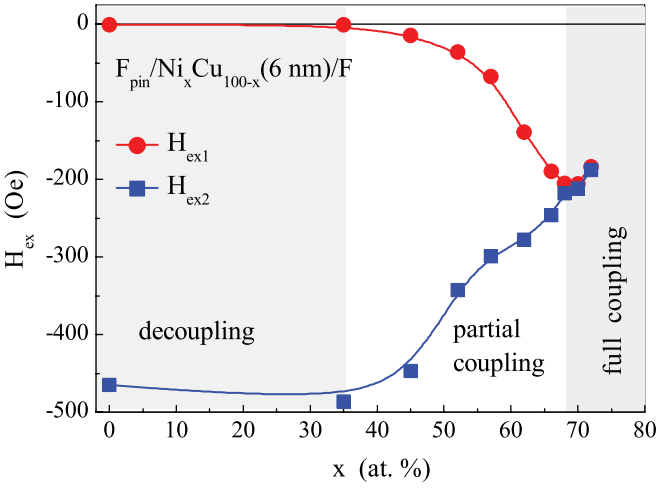

FIG. 4. (Color online) Exchange fields of the two outer ferromagnetic layers vs nickel concentration in a 6-nm-thick Ni-Cu spacer. The solid lines are guides to the eye.

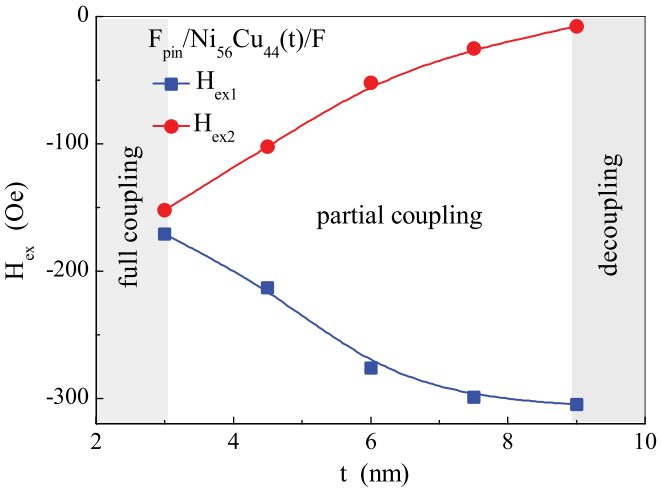

FIG. 5. (Color online) Exchange fields of the two outer ferromagnetic layers vs thickness of the Ni-Cu spacer for $x = 56$ at.% The solid lines are guides to the eye.

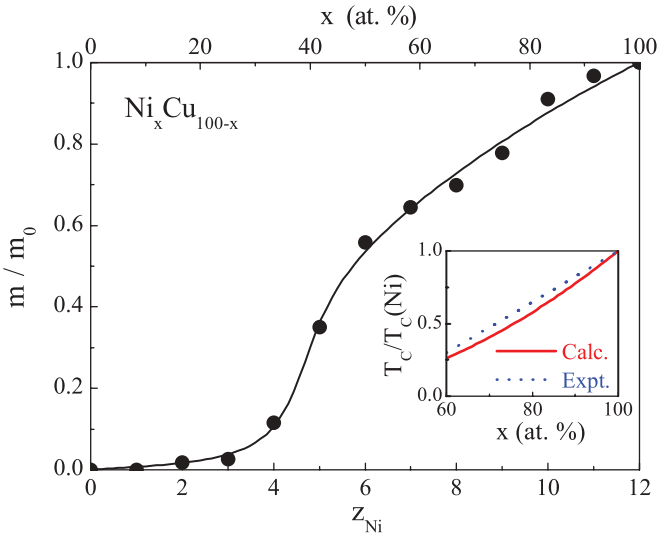

FIG. 6. (Color online) Calculated local atomic magnetic moment of Ni atoms in Ni_xCu_{100-x} alloys as a function of the number of the Ni atoms in the first coordination sphere, normalized to the moment of bulk fcc Ni of $m_0(\mathrm{Ni}) = 0.63\mu_B$. The solid lines are guides to the eye. Inset shows the calculated and experimental (Ref. 19) slopes of T_C in the bulk.

is a direct measure of the interlayer exchange coupling, while H_{ex2} additionally reflects the strength of the antiferromagnetic pinning. For $x > 70$ at.%, a bulk composition ferromagnetic at room temperature, minor and major loops merge into one (Fig. 2, red). Fine-stepping through the low-concentration range, illustrated by the minor loops in Fig. 3, shows that the onset of the interlayer exchange is at $x \approx 35$ at.%, which is due to the vanishing Ni atomic magnetic moment in the Cu matrix, as detailed below.

The dependence of the two exchange fields H_{ex1} and H_{ex2} on the Ni concentration in a 6-nm-thick Ni-Cu spacer is shown in Fig. 4. The free and pinned ferromagnetic layers are fully decoupled up to $x = 35$ at.% (red symbols), at which point H_{ex1} begins to increase in magnitude, first slightly and then substantially above 50 at.%, even though the spacer is still intrinsically paramagnetic at this concentration. At $x \approx 70$ at.% the two exchange fields merge into one (see Fig. 4, showing full coupling, which is expected since the spacer is intrinsically ferromagnetic at 70 at.% at RT.

Figure 5 shows the thickness dependence of the exchange fields for a nominally (in the bulk) paramagnetic spacer composition of $x = 56$ at.%. One can see that at 3 nm thickness the outer ferromagnetic layers are fully coupled and behave as one. For this composition, the interlayer exchange vanishes at approximately 9 nm in the spacer thickness. This is much greater than the interatomic spacing normally associated with direct exchange and indicates that the characteristic length scale for the induced ferromagnetic proximity effect under study is dictated by another mechanism, namely, thermally disordered lattice spins in the spacer by short-wave spin waves on length scales of at least several lattice units.

C. First-principles calculations

In order to understand the mechanism involved as well as optimize the performance of the material we develop a full model of the F/f(P)/F multilayer from first principles, which takes into account the thermal spin disorder as well as the effect of Cu dilution on the atomic magnetic moment of Ni in the performance-critical spacer layer.

For obtaining the dependence of the local atomic magnetic moment of Ni, $m_{loc}(z)$, on the number of the nearest-neighbor Ni atoms, z, the electronic structure of three special quasirandom superstructures,[30] which model random bulk Ni-Cu alloys, was calculated. The stoichiometries of the structures were $Ni_{25}Cu_{75}$, $Ni_{50}Cu_{50}$, $Ni_{75}Cu_{25}$. Figure 6 (solid circles) shows values of m_{loc} calculated by the FLAPW method. For calibration purposes, the slope of the Curie temperature of bulk Ni-Cu alloy was calculated and agreed well with the experiment,[19] as shown in the inset to Fig. 6. The interesting result in the obtained $m_{loc}(z)$ is that Ni becomes essentially nonmagnetic (diamagnetic) in the Ni-Cu alloy at a concentration of approximately 30 at.% Ni. This has important implications for optimizing the spacer material, as discussed below.

The key for efficient operation of a spin-thermoelectronic valve is the small width of its Curie transition. The green line in Fig. 7 shows the calculated magnetization per Ni atom of bulk $Ni_{80}Cu_{20}$ alloy. Blue and red colored data points show the calculated magnetization of the uniform (us) and gradient (gs) spacers as a function of temperature. Spacers are composed of 38 monolayers (approx. 7 nm) and placed between the plates of fcc Ni. At $T = 0$ K the magnetization is equal to the local moment of the Ni atom m_{loc} for this composition (Fig. 6). When the spacer is enclosed by strongly ferromagnetic outer electrodes (Ni), the ferromagnetic state becomes greatly extended in temperature, vanishing completely only above $0.9T_C$(Ni), as shown by the blue curve in Fig. 7. This means that the outer electrodes are strongly coupled at the nominal T_C of the spacer alloy (0.58), marked as the inflection point $M_t(T_t)$. The effective transition extends over the broad interval of $0.3T_C$(Ni)–$0.4T_C$(Ni). The reason for this extended transition is the strong ferromagnetic order induced in the spacer in

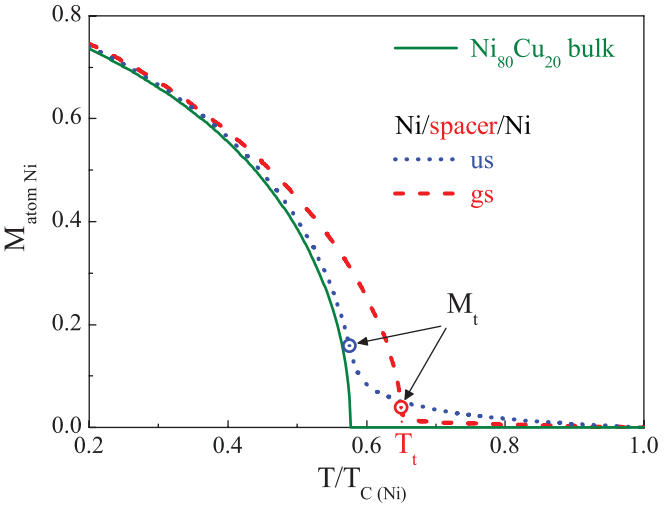

FIG. 7. (Color online) Calculated magnetization per nickel atom versus temperature for a bulk $Ni_{80}Cu_{20}$ alloy (green), uniform $Ni_{80}Cu_{20}$ (7 nm) (us, blue) and gradient $Ni_{65}Cu_{35}$(1 nm)/$Ni_{84}Cu_{16}$ (5 nm)/$Ni_{65}Cu_{35}$(1 nm) (gs, red) composition spacers enclosed by outer Ni layers. The inflection points, where the transition is steepest, as defined by the second derivative changing sign, are marked with $M_t(T_t)$.

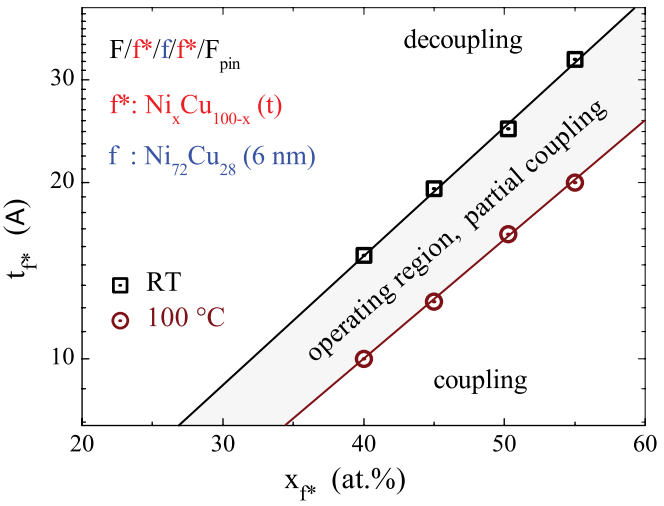

FIG. 9. (Color online) Thickness of the interfacial buffer layer f* of the weakly ferromagnetic spacer at which the outer Py layers decouple, as a function of its Ni content, for room temperature and 100 °C. The thickness and Ni concentration of the inner spacer layer f are 6 nm and 72 at.%, respectively. The solid lines are guides to the eye.

proximity to the interfaces, as shown in Fig. 8 with the open symbols, for two characteristic temperatures. At T_t the moment at the interface is enhanced fourfold compared to that in the center of the spacer, with a similar variation in the effective exchange and T_C across the thickness. The proximity length is an order of magnitude greater than the atomic spacing, so the induced magnetization penetrates all through the spacer thickness. The result is nonzero magnetic exchange between the outer ferromagnetic layers well above the intrinsic Curie point of the spacer material. This proximity effect should be

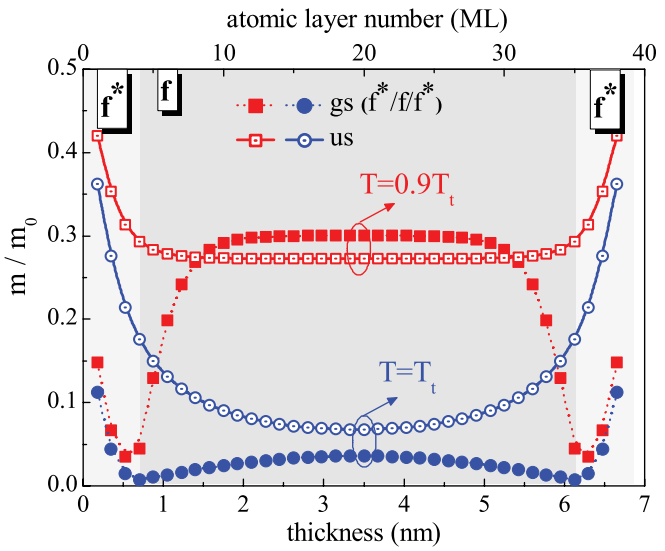

FIG. 8. (Color online) Calculated magnetization profiles in uniform $Ni_{80}Cu_{20}$(38 ML) (us, open symbols) and gradient $Ni_{65}Cu_{35}$ (4 ML)/$Ni_{84}Cu_{16}$(30 ML)/$Ni_{65}Cu_{35}$(4 ML) (gs, solid symbols) composition spacers for two different temperatures near the respective Curie points. ML indicates a monolayer.

universal for the F/f interface and sets a fundamental limitation on the width of the Curie transition of the weak ferromagnet incorporated in the multilayer.

It is highly desirable for device applications to narrow the magnetic transition in the spacer. Using the above detailed understanding of the highly nonuniform magnetization profile at F/f interfaces, we have designed a *gradient-spacer* design, in which the magnetic-atom concentration is reduced at the interfaces. This efficiently suppresses the proximity effect and makes the magnetization distribution much more uniform, as shown in Fig. 8, with solid symbols denoting a gradient spacer with the interface Ni concentration reduced from 80 to 65 at.%.

This change in the spacer layout has a dramatic effect on the simulated transition width, as shown in Fig. 7 (red). The magnetization at the inflection point is five times smaller for the gradient-spacer design, which translates into an order of magnitude sharper Curie transition for the trilayer, comparable in width with that for the ideal spacer (uniform, bulklike; green in Fig. 7).

D. Gradient spacer

In order to experimentally demonstrate the gradient-spacer effect proposed above, we have fabricated a range of valves, in which the spacer itself had a tri-layer structure f*/f/f*, with the buffer layers f* of different thickness and Ni content compared to the inner spacer layer f. The inner layer f had a fixed thickness and concentration of 6 nm and 72 at.%, respectively. This new layout is illustrated in the inset to Fig. 9, which shows the phase map of the resulting proximity effect. The vertical scale gives the thickness of the buffer layer f* for a given temperature, at which the outer Py layers fully decouple, determined in the same fashion as in Fig. 2. The phase map thus gives the operating region for a Curie valve based on the gradient-spacer design.

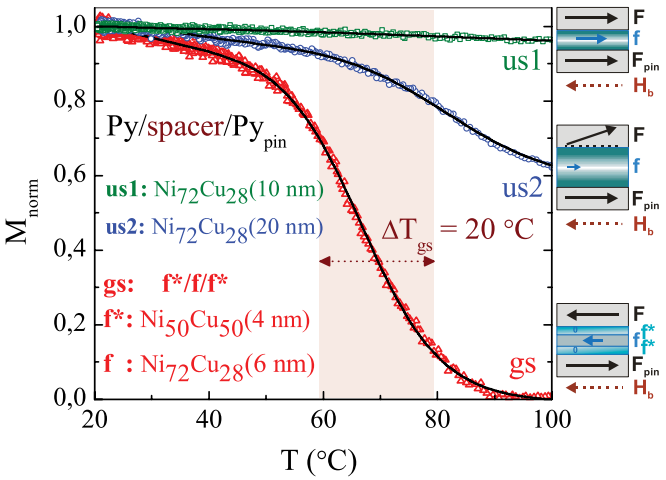

FIG. 10. (Color online) Normalized magnetization of two uniform $Ni_{72}Cu_{28}$ spacer multilayers, with spacers 10 (us1) and 20 (us2) nm thick, and a gradient $Ni_{50}Cu_{50}$(4 nm)/$Ni_{72}Cu_{28}$(6 nm)/$Ni_{50}Cu_{50}$ (4 nm) spacer (gs) multilayer. The solid lines are guides to the eye. The arrows in the illustrations of the right panel show the respective relative orientations of the magnetic moments in the center of the individual layers of the exchange-coupled F_{pin}/us(orgs)/F multilayer.

Interestingly, the scaling is logarithmic and shows that the thinnest layers decouple only below $x = 30$ at.%, where the Ni atoms become, in fact, nonmagnetic. We believe that this finding has high relevance for the RKKY interaction in this system in the thin-spacer limit studied previously experimentally[31,32] and theoretically.[33] The RKKY interlayer coupling through thin Cu spacers was interpreted to withstand paramagnetic Ni impurities up to approximately 35 at.% Ni, vanishing at higher concentrations. We suggest that the mechanism behind the strong RKKY coupling and its subsequent vanishing at higher Ni content was instead the loss of the atomic moment on Ni below 30 at.% Ni in Cu, detailed in our simulation results above (Fig. 6).

Having established the key physical parameters of the gradient-spacer design, below we demonstrate its greatly improved thermomagnetic characteristics. Figure 10 compares the temperature dependence of the magnetization of the two spacer layouts, with uniform and gradient-type composition. The samples were heated to 100 °C (to just above the bulk T_C of the inner spacer material, but below any significant reduction in the AF pinning), after which a reversing field bias H_b of −50 Oe was applied in the film plane opposite to the pinning direction (illustrated in Fig. 10), and the temperature was gradually decreased to room temperature while the magnetization was recorded. As a result, the spacer acts as an exchange spring of increasing strength, which rotates the free Py layer during the cooling from being along the biasing field toward the pinning direction.

The Curie transition (paramagnetic to ferromagnetic) is very broad in the uniform-spacer multilayer. In fact, the rotation of the free layer is far from complete at 100 °C, even for the relatively very thick spacer (20 nm), due to the residual proximity-induced interlayer exchange. In stark contrast, the gradient-spacer sample fully exchange-decouples into the antiparallel state of the outer Py layers at 90 °C (the Curie point of the inner spacer material with $x = 72$ at.%), and has a sharp transition into the parallel state of the multilayer on lowering temperature. The 20%–80% width of the transition is approximately 20 °C, the same as the full width at half maximum, and several times narrower than that for the uniform spacer. This result is in good agreement with the theoretically predicted behavior.

It is informative to note that the thermomagnetic switching demonstrated herein can have significant advantages over the recently developed and very promising thermally assisted switching, used in the memory technology based on thermal control of the antiferromagnetic exchange pinning.[34] One advantage is that the Curie point of a diluted ferromagnet can be easily varied in the desired range and is not fixed to the Néel (or blocking) temperature of the antiferromagnet. Furthermore, the ferromagnetic-to-paramagnetic transition typically is fully reversible and does not involve spin "blocking," and therefore should not suffer from training effects present at the exchange-biased F/AF interface.

IV. CONCLUSIONS

In conclusion, we have investigated strong/weak/strong ferromagnetic trilayers where the interlayer exchange coupling is controlled by driving the material through the Curie point of the spacer. The resulting exchange coupling between the strongly ferromagnetic outer layers can be switched on and off, or varied continuously in magnitude by controlling the temperature of the material. This effect is explained theoretically as due to induced ferromagnetism at F/f(P) interfaces. It is shown that the atomic magnetic moment and the effective interatomic exchange coupling are highly nonuniform throughout the spacer thickness, especially in proximity to the strongly ferromagnetic interfaces. This critically affects the interlayer exchange coupling and the ability to control it thermoelectronically. We have proposed and demonstrated a gradient-type spacer having a significantly narrower Curie transition and distinct thermomagnetic switching. The demonstrated multilayer material can form the base for a variety of magnetic devices based on spin-thermoelectronic switching.

ACKNOWLEDGMENT

We gratefully acknowledge financial support from EU-FP7-FET-Open through Project Spin-Thermo-Electronics.

*Corresponding author: vk@kth.se

[1] S. S. P. Parkin, Phys. Rev. Lett. **67**, 3598 (1991).
[2] A. Fert, P. Grünberg, A. Barthélémy, F. Petroff, and W. Zinn, J. Magn. Magn. Mater. **140–144**, 1 (1995).
[3] G. A. Prinz, Science **282**, 1660 (1998).
[4] U. Hartmann, *Magnetic Multilayers and Giant Magnetoresistance: Fundamentals and Industrial Applications* (Springer, Berlin, 1999).
[5] P. Grünberg, Phys. Today **54**(5), 31 (2001).

[6]C. Chappert, A. Fert, and F. Nguyen Van Dau, Nat. Mater. **6**, 813 (2007).
[7]J. M. Daughton, J. Magn. Magn. Mater. **192**, 334 (1999).
[8]J. S. Slonczewski, J. Magn. Magn. Mater. **159**, L1 (1996).
[9]E. B. Myers, D. C. Ralph, J. A. Katine, R. N. Louie, and R. A. Buhrman, Science **285**, 867 (1999).
[10]A. Brataas, A. D. Kent, and H. Ohno, Nat. Mater. **11**, 372 (2012).
[11]P. Grünberg, R. Schreiber, Y. Pang, M. B. Brodsky, and H. Sowers, Phys. Rev. Lett. **57**, 2442 (1986).
[12]G. Binasch, P. Grünberg, F. Saurenbach, and W. Zinn, Phys. Rev. B **39**, 4828 (1989).
[13]M. N. Baibich, J. M. Broto, A. Fert, F. Nguyen Van Dau, F. Petroff, P. Etienne, G. Creuzet, A. Friederich, and J. Chazelas, Phys. Rev. Lett. **61**, 2472 (1988).
[14]S. Andersson and V. Korenivski, IEEE Trans. Magn. **46**, 2140 (2010).
[15]S. Andersson and V. Korenivski, J. Appl. Phys. **107**, 09D711 (2010).
[16]A. M. Kadigrobov, S. Andersson, D. Radić, R. I. Shekhter, M. Jonson, and V. Korenivski, J. Appl. Phys. **107**, 123706 (2010).
[17]A. M. Kadigrobov, S. Andersson, Hee Chul Park, D. Radić, R. I. Shekhter, M. Jonson, and V. Korenivski, J. Appl. Phys. **111**, 044315 (2012).
[18]C. G. Robbins, H. Claus, and P. A. Beck, Phys. Rev. Lett. **22**, 1307 (1969).
[19]D. J. Chakrabarti, D. E. Laughlin, S. W. Chen, and Y. A. Chang, in *Phase Diagrams of Binary Copper Alloys*, edited by P. Subramanian, D. Chakrabarti, and D. Laughlin (ASM International, Materials Park, OH, 1994), p. 276.
[20]J. J. Hauser, Phys. Rev. **187**, 580 (1969).
[21]M. G. Samant, J. Stöhr, S. S. P. Parkin, G. A. Held, B. D. Hermsmeier, F. Herman, M. van Schilfgaarde, L.-C. Duda, D. C. Mancini, N. Wassdahl, and R. Nakajima, Phys. Rev. Lett. **72**, 1112 (1994).
[22]N. García and A. Hernando, J. Magn. Magn. Mater. **99**, L12 (1991).
[23]I. Navarro, M. Ortuno, and A. Hernando, Phys. Rev. B **53**, 11656 (1996).
[24]A. F. Kravets, A. N. Timoshevskii, B. Z. Yanchitsky, O. Yu. Salyuk, S. O. Yablonovskii, S. Andersson, and V. Korenivski, J. Magn. Magn. Mater. **324**, 2131 (2012); see also M. J. Fesharaki, L. Péter, T. Schucknecht, D. Rafaja, J. Dégi, L. Pogány, K. Neuróhr, É. Széles, G. Nabiyouni, and I. Bakonyi, J. Electrochem. Soc. **159**, D162 (2012) for a discussion of phase separation in electrodeposited Ni-Cu films.
[25]I. Bakonyi, E. Tóth-Kádár, J. Tóth, T. Becsei, T. Tarnóczi, and P. Kamasa, J. Phys.: Condens. Matter **11**, 963 (1999).
[26]R. E. Camley and D. R. Tilley, Phys. Rev. B **37**, 3413 (1988).
[27]H. C. Herper, E. Hoffmann, and P. Entel, Phys. Rev. B **60**, 3839 (1999).
[28]P. Blaha, K. Schwarz, G. Madsen, D. Kvasnicka, and J. Luitz, computer code WIEN2K (An Augmented Plane Wave + Local Orbitals Program for Calculating Crystal Properties) (Karlheinz Schwarz, Techn. Universität Wien, Austria, 2001).
[29]J. P. Perdew, K. Burke, and M. Ernzerhof, Phys. Rev. Lett. **77**, 3865 (1996).
[30]S. L. Shang, Y. Wang, D. E. Kim, C. L. Zacherl, Y. Du, and Z. K. Liu, Phys. Rev. B **83**, 144204 (2011).
[31]S. N. Okuno and K. Inomata, Phys. Rev. Lett. **70**, 1711 (1993).
[32]S. S. P. Parkin, C. Chappert, and F. Hermann, Europhys. Lett. **24**, 71 (1993).
[33]N. N. Lathiotakis, B. L. Györffy, E. Bruno, and B. Ginatempo, Phys. Rev. B **62**, 9005 (2000); N. N. Lathiotakis, B. L. Györffy, and J. B. Staunton, J. Phys.: Condens. Matter **10**, 10357 (1998); N. N. Lathiotakis, B. L. Györffy, J. B. Staunton, and B. Újfalussy, J. Magn. Magn. Mater. **185**, 293 (1998).
[34]I. L. Prejbeanu, M. Kerekes, R. C. Sousa, H. Sibuet, O. Redon, B. Dieny, and J. P. Nozières, J. Phys.: Condens. Matter **19**, 165218 (2007).